J|A|C|S ARTICLES

Published on Web 06/01/2010

On the Molecular and Electronic Structures of AsP_3 and P_4

Brandi M. Cossairt,[†] Christopher C. Cummins,*[,†] Ashley R. Head,[‡] Dennis L. Lichtenberger,*[,‡] Raphael J. F. Berger,[§] Stuart A. Hayes,[§] Norbert W. Mitzel,*[,§] and Gang Wu*[,⊥]

Department of Chemistry, Massachusetts Institute of Technology, 77 Massachusetts Avenue, Cambridge, MA-02139, Department of Chemistry and Biochemistry, The University of Arizona, 1306 East University Boulevard, Tucson, AZ-85721, Fakultät für Chemie, Universität Bielefeld, Universitätsstrasse 25, D-33615 Bielefeld, Germany, and Department of Chemistry, Queen's University, 90 Bader Lane, Kingston, Ontario, Canada K7L 3N6

Received March 27, 2010; E-mail: ccummins@mit.edu

Abstract: The molecular and electronic structures of AsP_3 and P_4 have been investigated. Gas-phase electron diffraction studies of AsP_3 have provided r_g bond lengths of 2.3041(12) and 2.1949(28) Å for the As−P interatomic distances and the P−P interatomic distances, respectively. The gas-phase electron diffraction structure of P_4 has been redetermined and provides an updated value of 2.1994(3) Å for the P−P interatomic distances, reconciling conflicting literature values. Gas-phase photoelectron spectroscopy provides experimental values for the energies of ionizations from the valence molecular orbitals of AsP_3 and P_4 and shows that electronically AsP_3 and P_4 are quite similar. Solid-state ^{75}As and ^{31}P NMR spectroscopy demonstrate the plastic nature of AsP_3 and P_4 as solids, and an extreme upfield ^{75}As chemical shift has been confirmed for the As atom in AsP_3. Finally, quantum chemical gauge-including magnetically induced current calculations show that AsP_3 and P_4 can accurately be described as strongly aromatic. Together these data provide a cohesive description of the molecular and electronic properties of these two tetraatomic molecules.

Introduction

Recently a directed metal-organic synthetic pathway for the synthesis of the binary interpnictogen compound AsP_3 has been developed.[1] AsP_3 has been found to be thermally stable over a wide temperature range, and the compound can be isolated in pure form.[1,2] AsP_3 has been studied in detail with respect to its electronic properties and its reactivity.[2] However, since no suitable single crystals for X-ray diffraction have yet been obtained, experimental structural data are only available for the coordination complexes $(AsP_3)Mo(CO)_3(P^iPr_3)_2$ and $[(AsP_3)FeCp^*(dppe)][BPh_4]$.[1,2] Due to its structural simplicity, thermal stability, heavy-atom composition, and volatility, AsP_3 is an ideal candidate for investigation by gas-phase electron diffraction (GED) and by gas-phase photoelectron spectroscopy.[3−5] Herein we report the determination of the structure of free molecules of AsP_3 in the gas phase, unbiased by solid-state intermolecular interactions. As well, for comparison, a reinvestigation of the gas-phase structure of elemental white phosphorus, i.e. P_4 molecules, is presented.[6] The electronic structures of neutral AsP_3 and P_4, and the energies associated with geometric distortion upon ionization of each substance have been probed by photoelectron spectroscopy. Solid-state nuclear magnetic resonance (NMR) investigations are provided to complement the gas-phase measurements by direct interrogation of the electronic environments of the arsenic atom (^{75}As NMR) and the phosphorus atoms (^{31}P NMR) in the solid state. Finally, quantum chemical methods are used to provide a more complete understanding of the electronic structure of AsP_3 through spherical aromaticity assessment via gauge-including magnetically induced current (GIMIC) calculations.[7,8]

Results and Discussion

Gas-Phase Electron Diffraction. Electron diffraction data were acquired for AsP_3 at a compound temperature of 110 °C and nozzle temperature of 115 °C. Figure 1b gives the reduced molecular scattering intensities and the radial distribution curve. C_{3v} symmetry was assumed for the structural refinement; hence, the geometry can be expressed in terms of two independent coordinates, which were chosen to be the P−P and the As−P

[†] Massachusetts Institute of Technology; synthesis.
[‡] The University of Arizona; photoelectron spectroscopy.
[§] Universität Bielefeld; gas-phase electron diffraction, QM and GIMIC calculations.
[⊥] Queen's University; solid-state NMR spectroscopy.

(1) Cossairt, B. M.; Diawara, M. C.; Cummins, C. C. *Science* **2009**, *323*, 602.
(2) Cossairt, B. M.; Cummins, C. C. *J. Am. Chem. Soc.* **2009**, *131*, 15501–15511.
(3) Cowley, J. M., Ed. *Electron Diffraction Techniques*; Oxford University Press: New York, 1992; Vols. 1 and 2.
(4) Weirich, T. E.; Labar, J. L.; Zou, X., Eds. *Electron Crystallography*; Springer: the Netherlands, 2006; Vol. 211.
(5) Hüfner, S. *Photoelectron Spectroscopy: Principles and Applications*; Springer: New York, 2003.
(6) Maxwell, L. R.; Hendricks, S. B.; Mosley, V. M. *J. Chem. Phys.* **1935**, *3*, 699–709.
(7) Taubert, S.; Sundholm, D.; Juselius, J.; Klopper, W.; Fliegl, H. *J. Phys. Chem. A* **2008**, *112*, 13584–13592.
(8) Juselius, J.; Sundholm, D.; Gauss, J. *J. Chem. Phys.* **2004**, *121*, 3952–3963.

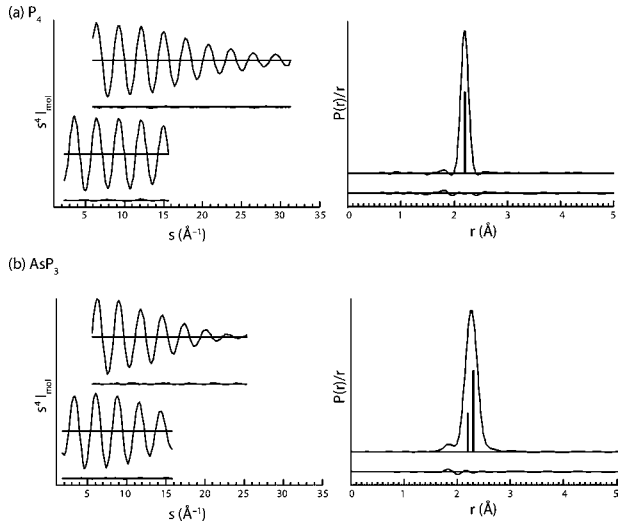

Figure 1. Molecular scattering intensities and radial distribution curves for P_4 and AsP_3.

distances. The two structural parameters were refined together and independently (as an average value and a difference), while the two interatomic vibrational amplitudes were restrained to a fixed ratio relative to the values predicted by *ab initio* calculations (see Experimental Section for further details). The P−P and the As−P distances were determined to be 2.1949(28) and 2.3041(12) Å (r_g structure type, all experimental distances from this study are given with uncertainties of 1σ).

Examination of the P−P and P−As interatomic distances in the previously obtained single-crystal X-ray diffraction structures of transition metal−AsP_3 adducts give As−P bond lengths ranging from 2.306(6) to 2.336(2) Å (distances to the nonmetal-bound P atom) and P−P bonds ranging from 2.165(8) to 2.231(3) Å (distances to the non metal-bound P atom).[1,2] Our values obtained from the gas-phase structure are in good agreement with these solid-state data. For comparison, single bond distances calculated using covalent radii are 2.32 Å for As−P and 2.22 Å for P−P.[2,9] The P−As−P and the P−P−As angles, which are dependent parameters, were determined to be 56.89(11)° and 61.56(5)°. Calculations predict that both interatomic vibrational amplitudes (P−P and As−P) are equal within reasonable accuracy, and they were refined to a value of 0.06(2) Å.

For comparison with the structure of AsP_3 it was desirable to have access to a precise gas-phase structure of free P_4 molecules. However, despite its structural simplicity, various and partly contradicting results about the molecular structure of free P_4 have been published, the most recent one as late as 1999.[10] There is only one GED investigation of P_4 to be found in the literature which stems from 1935.[6] In this study no rotating sector[11] was used. We recently demonstrated that such investigations, despite all merits regarding the relative accuracy bearing in mind the archaic simplicity of employed techniques, yield in cases only very limited absolute accuracies.[12] For these reasons we undertook, parallel to the study of AsP_3, also a reinvestigation of the gas-phase structure of P_4 by means of electron diffraction. Molecular scattering intensities and the radial distribution curve is given in Figure 1a. At a nozzle temperature of 100 °C, we acquired diffraction data which resulted, by using a T_d-symmetric one-parameter model, in an r_g distance of 2.1994(3) Å between the P atoms and an interatomic vibrational amplitude of 0.0560(5) Å. It is also worthy to compare this new value to those obtained from structures of P_4 in other phases. For example, values extracted from X-ray diffraction experiments of P_4 in the liquid phase at 321 and 499 K provided a P−P bond length of $r_{av} = 2.25$ Å.[13,14] In the solid state, single-crystal X-ray diffraction of the β-P_4 phase, crystallized from CS_2 solution, gives an average value of 2.182(5) Å (range 2.175(5) to 2.192(5) Å) as determined from 18 P−P bond lengths of three crystallographically independent molecules, which was further corrected for libration to a value of 2.204 Å (range 2.199 to 2.212 Å).[15]

In 1997 Persson et al. estimated the basis set limit at the nonrelativistic CCSD(T) level of theory for the equilibrium P−P distance r_e to 2.186(1) Å, while they achieved a value of 2.188 Å using an ANO type basis set of the contraction form [6s11p4d3f1g].[16] Now we could verify this estimation of the basis set limit at the explicitly correlated CCSD(T)-F12/aug-cc-pCVQZ level of theory[17] including all electrons into the correlation space, in yielding an r_e value of 2.1860 Å for P−P in P_4. Remarkably, core electron correlation affects the calculated P−P distance significantly by shortening it by approximately 1 pm compared to the result from taking only valence electrons into the correlation space (2.194 Å).

The experimental structures give r_g P−P bond lengths for AsP_3 and P_4 that are equal within three standard deviations: AsP_3 [2.192−2.198 Å], P_4 [2.198−2.200 Å]. The best theoretically obtained values for P−P interatomic distances are 2.186 Å for P_4[16] and 2.212 Å for AsP_3,[2] while a value of 2.328 Å has been predicted for the As−P interatomic distance. In order to allow a comparison of these equilibrium distances (r_e) with our experimental (r_g) values, one would have to estimate a distance correction for ro-vibrational effects at the experimental temperature. In principle this can be attempted using calculated anharmonic force fields, leading in our case to corrections of the magnitude 0.003 Å (to be subtracted from the r_g values). However, great care is suggested using such corrections, as the literature discussing the earlier gas-phase structure determination of P_4 by means of high-resolution IR spectroscopy[10] in comparison with the calculated r_e values mentions problems with highly excited rotational states and difficulties in estimating reliable distance corrections. As this problem has not been resolved thus far, we abstain from such a direct comparison using corrections of unknown reliability in these particular cases.

Photoelectron Spectroscopy and Electronic Structure. Gas-phase photoelectron spectroscopy directly probes the electronic structure of molecules.[5,18] In order to understand the photoelectron spectrum and the electronic structure of AsP_3, it is useful to start with a summary of P_4, previously reported by

(9) Pyykkö, P.; Atsumi, M. *Chem.—Eur. J.* **2009**, *15*, 186–197.
(10) Boudon, V.; Mkadmi, E. B.; Bürger, H.; Pierre, G. *Chem. Phys. Lett.* **1999**, *305*, 21–27.
(11) Tremmel, J.; Hargittai, I., Eds. *Stereochemical Applications of Gas-Phase Electron Diffraction*; Methods in Stereochemical Analysis, Vol. A, The Electron Diffraction Technique; VCH Publishers Inc.: Deerfield Beach, FL, 1988; Chapter 6.
(12) Berger, R. J. F.; Mitzel, N. W. *J. Mol. Struct.* **2010**, DOI: 10.1016/j.molstruc.2010.02.018.
(13) Thomasand, C. D.; Gingrich, N. S. *J. Chem. Phys.* **1938**, *6*, 659.
(14) Gingrich, N. S. *Rev. Mod. Phys.* **1943**, *15*, 90–110.
(15) Simon, A.; Borrmann, H.; Horkah, J. *J. Chem. Ber.* **1997**, *130*, 1235.
(16) Persson, B. J.; Taylor, P. R.; Lee, T. J. *J. Chem. Phys.* **1997**, *107*, 5051–5057.
(17) Werner, H.-J.; et al. *MOLPRO*, v. 2008.1; Institut für Theoretische Chemie, Universität Stuttgart: Stuttgart, FRG, 2009; http://www.molpro.net.
(18) Turner, A. R. *Philos. Trans. R. Soc.* **1970**, *268*, 7–31.

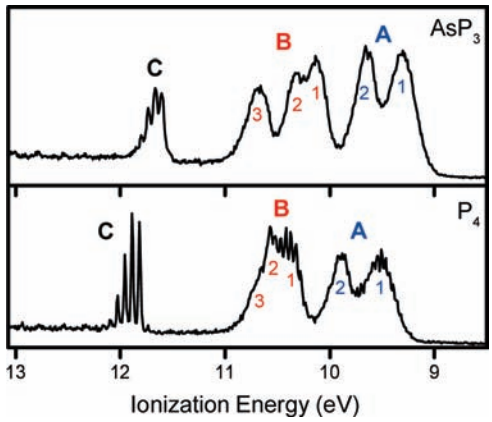

Figure 2. He I photoelectron spectra of AsP_3 (top) and P_4 (bottom).

Table 1. Vertical Ionization Energies of P_4 and AsP_3

	peak position (eV)	
peak	P_4	AsP_3
A(1)	9.52	9.30
A(2)	9.90	9.66
B(1)	10.35	10.13
B(2)	10.54	10.35
B(3)	10.86	10.68
C	11.89	11.67

Wang et al.[19,20] The valence photoelectron spectra of AsP_3 and P_4 are compared in Figure 2. The highest occupied orbitals of P_4 are $...(2a_1)^2(2t_2)^6(e)^4$. When an electron is ionized from the HOMO *e* orbital, an ^2E state is formed which couples with the $\upsilon_2(e)$ vibration causing a Jahn−Teller distortion in the cation. The ^2E state can also be split by spin−orbit coupling. The first two ionization peaks of P_4, labeled **A(1)** and **A(2)** in the photoelectron spectrum shown at the bottom of Figure 2, are the result of ionization from this *e* symmetry orbital, and they have an observed splitting energy of 0.38 eV. This splitting is primarily the result of the Jahn−Teller reduction in symmetry since the spin−orbit coupling of the valence ionizations of the P atom is on the order of only 0.04 eV.[21] The next band in the spectrum, labeled **B** in the figure, contains three components that begin as the $2t_2$ set in the neutral molecule. Upon ionization, the two different effects again combine to remove the triple degeneracy of the $^2T_2$ state. The Jahn−Teller distortion, due to mostly the $\upsilon_3(t_2)$ vibration, splits the $2t_2$ orbitals into three components in the cation. Since the splitting energies are larger than 0.04 eV, Jahn−Teller effects are again the dominant reason for the splitting. The last peak at 11.9 eV (labeled **C**) is the $^2A_1$ cationic state and shows vibrational fine structure due to the $\upsilon_1(a)$ symmetric vibration with a frequency spacing of 554(11) cm^{-1}.

The photoelectron spectrum of AsP_3 is shown at the top of Figure 2. It contains features similar to those of the spectrum for P_4, though most of the peaks are shifted to lower ionization energies, as seen in Table 1, and there is a greater spread of ionizations in band **B**. With the replacement of one P atom with a less electronegative As atom, the molecular orbitals should be easier to ionize. The vibrational structure is not as resolved as in the P_4 spectrum except for peak **C**. This is largely due to lower-frequency vibrations that result in smaller vibrational spacings that are comparable to the instrument resolution. The T_d symmetry is lowered to C_{3v}, and the symmetries of the highest occupied molecular orbitals of the neutral molecule change to $...(3a_1)^2(4a_1)^2(2e)^4(3e)^4$. The doublet in the **A** ionization band arises again from the Jahn−Teller distortion with the same splitting energy as that in the P_4 spectrum.

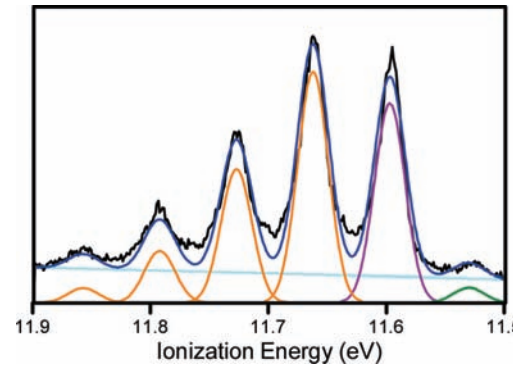

Figure 3. The vibrational progression of the symmetric stretch in the He I photoelectron spectrum of AsP_3. The leading green band corresponds to a hot band transition. The purple band is the reference peak; the progression in yellow was generated by a Poisson distribution with a frequency of 523(9) cm^{-1} and a Huang−Rhys factor of 1.15(2).

The major difference in appearance between the spectra of AsP_3 and P_4 occurs in band **B**. In the AsP_3 spectrum, the highest energy component in band **B** is a distinct peak instead of a shoulder as observed for P_4. A lowering of molecular symmetry to C_{3v} splits the $2t_2$ triple degeneracy that occurs in P_4 into the $4a_1$ and $2e$ orbitals in the neutral molecule of AsP_3. This removal of degeneracy in the neutral molecule and before ionization is in contrast to that of P_4 where the lifting of the degeneracy occurs in the cation. The peaks labeled **B(1)** and **B(2)** are a result of a Jahn−Teller distortion and spin−orbit coupling, but the spin−orbit coupling is slightly larger in this system. The spin−orbit coupling constant of the As neutral atom and monopositive ion is 0.20 eV.[22] This increase from about 0.04 eV for the P atom results in a spin−orbit coupling constant of about 0.08 eV on average for the molecule, assuming completely delocalized orbitals for AsP_3, and is reflected in the increase of the splitting between the two lower energy components from 0.19 to 0.22 eV.

Clear vibrational structure outlines the peak at 11.75 eV and is analyzed with a Poisson distribution in Figure 3. The spacing of the vibrational progression indicates a vibrational frequency of 523(9) cm^{-1}, corresponding to a symmetric stretch of the atoms. This frequency is smaller than 554(11) cm^{-1}, that of P_4, as expected from the greater mass of As, but the Huang−Rhys distortion factor of 1.15(2) is the same. The similarity in this vibrational structure between the two molecules further illustrates similarities in electronic structure.

Our recently published DFT calculations agree well with the photoelectron spectra of P_4 and AsP_3.[2] A comparison of the separation of Kohn−Sham orbitals with the separation of the peaks in the photoelectron spectra shows that the DFT calculations accurately model the electronic structure of the molecules. For peaks affected by the cationic Jahn−Teller distortion and spin−orbit coupling, an average peak position is used for

(19) Wang, L. S.; Niu, B.; Lee, Y. T.; Shirley, D. A.; Ghelichkhani, E.; Grant, E. R. *J. Chem. Phys.* **1990**, *93*, 6318–6326.
(20) Wang, L. S.; Niu, B.; Lee, Y. T.; Shirley, D. A.; Ghelichkhani, E.; Grant, E. R. *J. Chem. Phys.* **1990**, *93*, 6327–6333.
(21) Ishiguro, E.; Kobori, M. *J. Phys. Soc. Jpn.* **1967**, *22*, 263–270.
(22) Wittel, K.; Manne, R. *Theor. Chim. Acta* **1974**, *33*, 347–349.

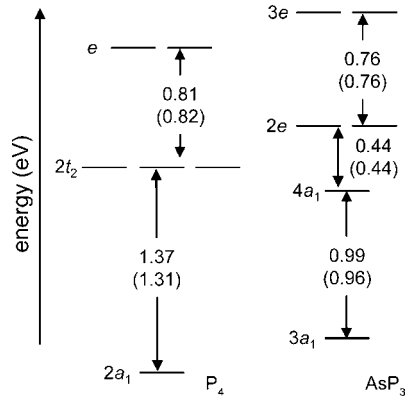

Figure 4. Energy level diagram for both AsP_3 and P_4. The top number is the experimental splitting (averaged for the split ionization bands) obtained from the photoelectron spectroscopy data and the bottom number in parentheses is the splitting of Kohn−Sham orbital energies as obtained from DFT calculations.

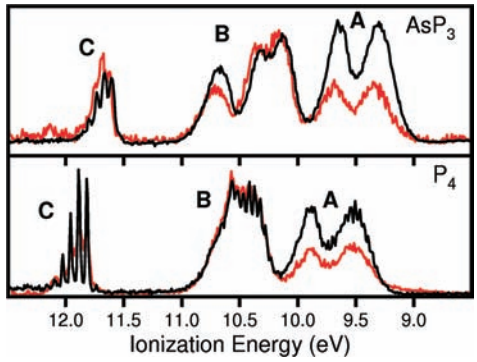

Figure 5. Comparison between He I (black) and He II (red) photoelectron spectra for both AsP_3 and P_4.

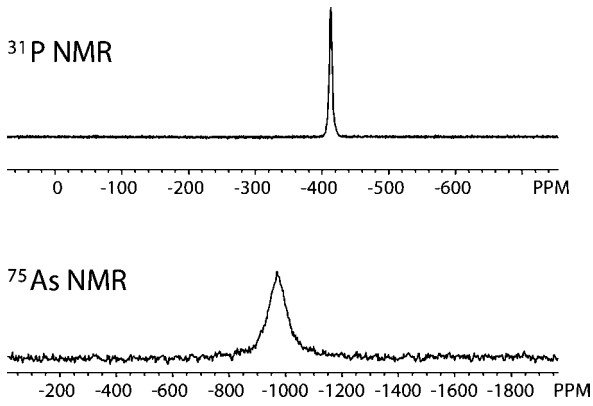

Figure 6. Solid-state NMR spectra of AsP_3 obtained at 14.09 T.

comparison to the calculated values. Figure 4 compares the experimental and calculated orbital separations in an energy level diagram.

Insight into the atomic character of the molecular orbitals is routinely obtained by observing changes in the relative intensities of the ionization bands with the change from He I (21.22 eV) to He II (40.81 eV) source photon energies.[5] In this case the cross-section for ionization of As 4p electrons decreases by a factor of 5 more than the cross section for ionization of P 3p electrons from He I to He II excitation. Hence, in comparing the relative He I to He II ionization intensity changes for AsP_3 and P_4, ionizations that have greater As 4p character should decrease substantially in relative intensity compared to ionizations that have greater P 3p character. Figure 5 illustrates the change in He I and He II ionization intensities for AsP_3 and P_4, and Table 2 lists the ratios of the He II to He I integrated peak areas for each ionization band of both molecules with the area of band **A** being the reference. For the comparison in Table 2 the ionizations between 10 to 11 eV are grouped into a single region **B** because for P_4 the vibrational manifolds of the ionizations in this region are overlapped into a single band. This overlap of the ionizations is conducive to vibronic and spin−orbit mixing of the electronic states, and the individual ionization intensities cannot be independently determined. The lack of visible change in the overall contour of this band from He I to He II excitation is suggestive of the mixing of these states in the ionization process. In contrast, as mentioned previously, the energy spread of these states is greater for AsP_3, such that separate ion states are observed with relative intensity changes between He I and He II excitation. The important point shown in Table 2 is that the change in integrated intensity of the ionizations in region **A** relative to the integrated intensities in regions **B** and **C** is the same for both molecules. This consistency indicates that the electrons are extremely delocalized throughout all of the valence molecular orbitals of these molecules.

Table 2. Ratios of the Peak Areas from the He I and the He II Photoelectron Spectra of Both Compounds Normalized to the Area of Peak **A**

	He II/He I peak area ratio	
ionization band	P_4	AsP_3
A	1	1
B	1.90	1.93
C	2.60	2.40

Table 3. Comparison of the Isotropic ^{31}P Chemical Shifts between P_4 and AsP_3 in Different Environments

molecule	$\delta_{iso}(^{31}P)$/ppm	molecule	$\delta_{iso}(^{31}P)$/ppm
$P_4(g)_{exptl}$	−551.5[a]	$AsP_3(g)_{exptl}$	−
$P_4(g)_{calc}$	−530[b]	$AsP_3(g)_{calc}$	−492[b]
P_4(benzene solution)	−520[c]	AsP_3(benzene solution)	−484[c]
P_4(l)	−460[a]	AsP_3(l)	−
P_4(s)	−	AsP_3(s)	−413

[a] From ref 24. [b] The ^{31}P chemical shift (δ) was converted from the computed shielding constant (σ) using the absolute ^{31}P shielding scale: $\delta = 328.35 - \sigma$.[25] [c] From ref 2.

Solid-State Nuclear Magnetic Resonance. Figure 6 shows the solid-state ^{75}As and ^{31}P NMR spectra obtained at 14.09 T for a stationary powder sample of AsP_3 at 298 K. The fact that a single sharp peak was observed in each of these NMR spectra immediately suggests that AsP_3 molecules undergo rapid reorientation (or jumps) in the solid state at this temperature. This plastic crystal phase behavior of AsP_3 was observed at temperatures above 213 K. It is well-known that above 196.3 K P_4 is also in a plastic crystal phase.[23] The observed ^{31}P chemical shift for solid AsP_3, −413 ppm, is quite different from that measured in benzene solution, −484 ppm.[2] In fact, as seen from Table 3, the ^{31}P chemical shifts of P_4 and AsP_3 exhibit strong dependence on the chemical environment of the molecules.[24,25] The ^{75}As chemical shift observed for solid AsP_3, −962 ppm, is the most negative value (corresponding to the

(23) Boden, N.; Folland, R. *Mol. Phys.* **1971**, *21*, 1123–1139.

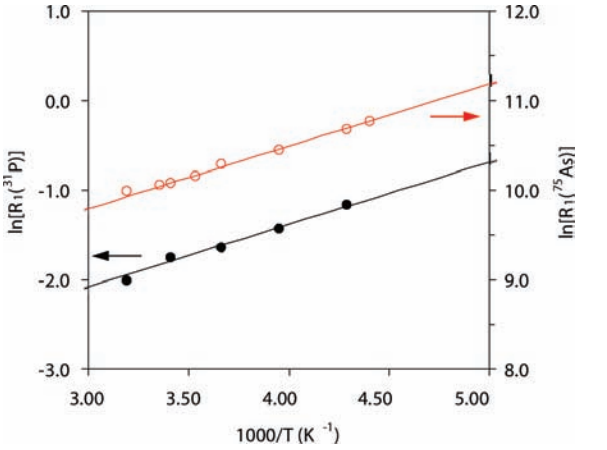

Figure 7. Variable-temperature ^{75}As and ^{31}P spin−lattice relaxation data obtained for solid AsP_3.

most shielded environment at the ^{75}As nucleus) among all known arsenic compounds.[26]

To learn more about the molecular dynamics of AsP_3 in the solid state, we determined the spin−lattice relaxation times (T_1) for both ^{75}As and ^{31}P nuclei at temperatures between 213 and 313 K. At 14.09 T, the relaxation mechanism for ^{31}P is predominantly the chemical shift anisotropy. On the other hand, the relaxation mechanism for ^{75}As ($I = 3/2$) is the quadrupolar interaction. Similar to the case of P_4, the molecular jumps of AsP_3 in the plastic crystal phase satisfy the extreme narrowing condition,[27] i.e., $\omega_0\tau \ll 1$ where ω_0 is the Larmor angular frequency of the nucleus under observation and τ is the correlation time for molecular reorientation. We were able to analyze simultaneously the ^{75}As and ^{31}P T_1 data shown in Figure 7. Our analysis yields the following parameters for AsP_3 reorientation dynamics: $\tau = \tau^0 \exp(E_a/RT)$ where $\tau^0 = 3.1 \times 10^{-13}$ s and $E_a = 5.8$ kJ mol^{-1}. These parameters compare well with those reported for P_4 ($\tau^0 = 4.7 \times 10^{-13}$ s and $E_a = 5.7$ kJ mol^{-1}).[23] The same T_1 analysis also yields two important NMR parameters: $\Delta\sigma(^{31}\mathrm{P}) = \sigma_{33} - \sigma_{11} = 400 \pm 10$ ppm, and $C_Q(^{75}\mathrm{As}) = 42 \pm 2$ MHz, assuming that both the ^{31}P shielding tensor and the ^{75}As quadrupole coupling tensor are axially symmetric. The observed ^{31}P shielding anisotropy for solid AsP_3 is in excellent agreement with that measured for P_4, $\Delta\sigma(^{31}\mathrm{P}) = 405$ ppm.[28]

Aromaticity Considerations. According to nuclear independent chemical shielding calculations (NICS),[29] AsP_3 possibly shows similarly strong (spherical) aromaticity when compared with P_4.[30] However, in order to assign a reference point in space at which the NICS value will be calculated, either one point in space can be determined uniquely according to molecular symmetry (the symmetry center in the case of P_4) or some more or additional considerations have to be taken into account. In previous analyses[2] the cage critical point of AsP_3 was used as a reference point for the NICS calculation. Since there is no obvious direct physical connection of these properties, we undertook further investigations to quantify and compare the degree of aromaticity of P_4 and AsP_3.

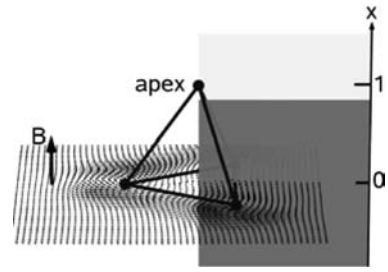

Figure 8. Relative orientation of the magnetic field (**B**) and the molecules used in the GIMIC calculations. The molecules are oriented in way that the apex-atom to center-of-gravity vector is parallel to the magnetic field. Some representative current density vectors in a plane orthogonal to the magnetic field vector and slightly below the P_3 ring plane are shown. The larger current density vectors in this plane outside the molecule describe a strong diamagnetic circular ring current. In order to determine the strength of the total current density induced, the current density vectors were integrated through planes (dark and light gray areas) extending from 10 Å below the P_3 ring plane ($x = 0$) up to 3 Å above the apex atom. The total current densities per magnetic field strength (dI/dB) are 49 nA/T for P_4 and 81 nA/T for AsP_3. In order to simplify comparisons the x-units were scaled for both molecules in a way that the apex atom lies at $x = 1$.

GIMIC[8,31] calculations have been performed using electron densities calculated at the DFT level of theory (see Computational Details) in order to calculate a magnetically induced current density field for P_4 and AsP_3. The magnetic field was oriented parallel to the center of the gravity apex-atom vector as shown in Figure 8. Some representative current density vectors in a plane orthogonal to the magnetic field vector and slightly below the P_3 ring plane are shown in Figure 8. The larger current density vectors in this plane outside the molecule describe a strong diamagnetic circular ring current. In order to determine the strength of the total current density induced, the current density vectors were integrated through planes (dark- and light-gray areas in Figure 8) extending from 10 Å below the P_3 ring plane up to 3 Å above the apex atom. The total current densities per magnetic field strength (dI/dB) are 49 nA/T for P_4 and 81 nA/T for AsP_3.

Since the integration plane passes through half the apex atoms a large contribution to the total current density is given by their closed subshells (each closed shell is equivalent to a spherical aromatic system).[8,31] In order to estimate the amount of ring current which does not stem from the apex atoms, the x derivative of the integrated currents was (numerically) formed, yielding a local density contribution function. The local minima of these functions x_{min} (marked in Figure 9 with the base of bold vectors) correspond in a sense to a region where the apex-atoms contributions to the current just balance the contribution from the rest of the molecule. Hence the total currents integrated from $-\infty$ (here numerically approximated by -10 Å) up to x_{min} can be taken as the apex atom independent ring current. These values are 29 and 17 nA/T for P_4 and AsP_3. Hence the situation is the reverse of that compared to complete induced ring current values. Our calculations suggest that both compounds can be regarded as strongly aromatic (benzene shows approximately values between 10 and 11 nA/T weakly depending on the level of theory employed to calculate the electron density);[8,31]

(24) Heckmann, G.; Fluck, E. *Mol. Phys.* **1972**, *23*, 175–183.
(25) Jameson, C. J.; De Dios, A.; Jameson, A. K. *Chem. Phys. Lett.* **1990**, *167*, 575–582.
(26) Balimann, G.; Pregosin, P. S. *J. Magn. Reson.* **1977**, *26*, 283–289.
(27) Keeler, J. *Understanding NMR Spectroscopy*; John Wiley & Sons Ltd.: West Sussex, 2005.
(28) Spiess, H. W.; Grosescu, R.; Haeberlen, U. *Chem. Phys.* **1974**, *6*, 226–234.
(29) Schleyer, P. V.; Maerker, C.; Dransfeld, A.; Jiao, H. J.; van Eikema Hommes, N. *J. Am. Chem. Soc.* **1996**, *118*, 6317–6318.
(30) Hirsch, A.; Chen, Z. F.; Jiao, H. J. *Angew. Chem., Int. Ed.* **2001**, *40*, 2834–2838.
(31) Johansson, M. P.; Juselius, J.; Sundholm, D. *Angew. Chem., Int. Ed.* **2005**, *44*, 1843–1846.

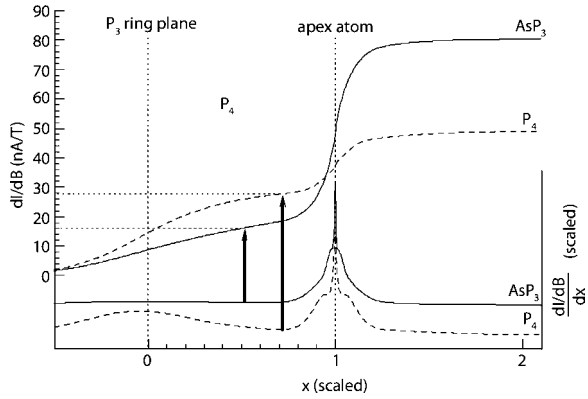

Figure 9. Two upper curves show the current densities integrated over rectangular regions from 10 Å below the P_3 ring plane to x (see Figure 2 for a description of the x coordinate) for P_4 (dotted line) and AsP_3 (full line). In order to determine the local current contributions from a certain x level in the molecule, the numerical derivatives of the current density integral curves by the x are determined (two lower curves). The integrated current densities up to these local minima of the derivatives (origins of bold vectors) may be taken as an estimate of the fraction of the total spherical current originating only from the P_3 ring. This excludes the contribution of the apex atom (29 nA/T for P_4 and 17 nA/T for AsP_3), which contributes by itself to a big fraction of the total aromatic current, due its filled subshells (visible in the derivative curves around $x = 1$).

however, AsP_3 shows distinctly lower magnetically induced current densities flowing through the bond cage than is the case for P_4.

Conclusions

Several new features of AsP_3 have been brought to light with this series of investigations. First, the molecular structure has been determined in the gas phase, free of solid-state packing effects, giving an As−P bond length of 2.3041(12) Å and a P−P bond length of 2.1949(28) Å. The myriad of contradictory structures of P_4 that have been described in the literature required a reevaluation of the P_4 gas-phase structure.[6,32,33] A quote from Denk et al. that speaks to this point is as follows, "Bond distances of P_4 obtained in our group with large basis sets ... are in excellent agreement with Haser's results and give further support to his suggestion that the structure of P_4, in particular the gas-phase electron diffraction structure which dates from 1935, should be reexamined".[32,34] Denk et al. further state that the experimental values of the P−P bond lengths of 2.22 and 2.21 Å disagree with their high-level calculations which give $r_e = 2.198$ Å. The updated value reported here of $r_g = 2.1994(3)$ Å directly addresses and reconciles this issue. Second, the ionization energies of the valence molecular orbitals have been determined using photoelectron spectroscopy showing that the HOMO of AsP_3 is more accessible by 0.3 eV when compared with P_4 and show that overall the two molecules are electronically very similar. Further, the comparison of He I and He II photoelectron spectra has shown that the valence electrons in AsP_3 and P_4 are strongly delocalized for both molecules. Solid-state NMR data has demonstrated the plasticity of AsP_3 in the solid state and has shown that the ^{75}As nucleus in AsP_3 is the most shielded of known arsenic nuclei. Finally, GIMIC calculations have confirmed that AsP_3 can be thought of as strongly aromatic; however, significantly less magnetically induced current flows through the bond cage when compared with that with P_4. The data reported herein provide a more complete understanding of the fundamental physical properties of these tetrahedral, elemental entities and beckon further development of the molecular chemistry of group 15 elements.

Experimental Section

AsP_3 was prepared as described previously and was sublimed prior to analysis in all cases.[1,2]

Gas-Phase Electron Diffraction. Electron scattering intensities for P_4 and AsP_3 were recorded at 100 and 110 °C sample temperature and 110 and 115 °C nozzle temperature using a newly constructed high temperature nozzle and reusable Fuji imaging plates on a Balzers KD-G2 Gas-Eldigraph in Bielefeld[35] (formerly operated in Tübingen by H. Oberhammer), equipped with a new electron source (STAIB Instruments), operating at ca. 60 kV and with a beam current of ∼200 nA. During data acquisition the background pressure rose from 1.3×10^{-6} to 2.5×10^{-5} mbar, and the optimal exposure time was 15 to 20 s. Exposed imaging plates were scanned using a commercially available Fuji BAS 1800 scanner, yielding digital 16-bit gray-scale image data. The image data were reduced to total intensities using T. G. Strand's program PIMAG[36] (version 040827) in connection with a sector curve, which is based on experimental xenon diffraction data and tabulated scattering factors of xenon. Further data reduction (yielding molecular-intensity curves), the molecular structure refinement, and the electron wavelength determination (from benzene data) were performed using version 2.4 of the ed@ed program.[37] The scattering factors employed were those of Ross et al.[38] Further details about the Bielefeld GED apparatus and methods are published previously.[35] Data analysis parameters for each compound and each data set including R-factors (R_D and R_G), scale factors, correlation parameter values, data ranges, weighting points, nozzle-to-plate distances, and electron wavelengths are given in the Supporting Information.

Photoelectron Spectroscopy. Gas-phase photoelectron spectra (He I and He II) were recorded on an instrument built around a 36 cm radius, 8 cm gap hemispherical analyzer[39] (McPherson) using a custom-designed photon source and collection methods.[40,41] Instrument control and electron counting are interfaced to a National Instruments USB-6251 multifunction DAQ board and custom software. Samples sublimed cleanly at room temperature from a Young's tube with no evidence of decomposition. The argon $^2P_{3/2}$ ionization at 15.759 eV was used as an internal calibration lock of the absolute ionization energy, and its difference with the CH_3I $^2E_{1/2}$ ionization at 9.538 eV provided an external calibration of the energy scale. The instrument resolution (measured as the full width at half-maximum (fwhm) of the argon $^2P_{3/2}$ ionization) was 0.020−0.028 eV during data collection. The He I spectra were corrected for the He Iβ line (1.866 eV higher in energy and 3% the intensity of the He Iα line), and the He II spectra were corrected for the He IIβ line (7.568 eV higher in energy and 12% the intensity of the He IIα line). All data also were intensity corrected with an

(32) Denk, M. K.; Hezarkhani, A. *Heteroat. Chem.* **2005**, *16*, 453–457.
(33) Corbridge, D. E. C.; Lowe, E. J. *Nature* **1952**, *170*, 629.
(34) Häser, M.; Treutler, O. *J. Chem. Phys.* **1995**, *102*, 3703–3711.
(35) Berger, R. J. F.; Hoffmann, M.; Hayes, S. A.; Mitzel, N. W. *Z. Naturforsch. B* **2009**, *64*, 1259–1268.
(36) Gundersen, S.; Samdal, S.; Strand, T. G.; Volden, H. V. *J. Mol. Struct.* **2007**, *832*, 164–171.
(37) Hinchley, S. L.; Robertson, H. E.; Borisenko, K. B.; Turner, A. R.; Johnston, B. F.; Rankin, D. W. H.; Ahmadian, M.; Jonesc, J. N.; Cowley, A. H. *Dalton Trans.* **2004**, 2469–2476.
(38) Ross, A. W.; Fink, M.; Hilderbrandt, R. *International Tables for Crystallography*, Vol. C (Ed.: A. J. C. Wilson), Kluwer, 1992, p 245.
(39) Siegbahn, K.; Nordling, C.; Fahlman, A.; Nordberg, R.; Hamrin, K.; Hedman, J.; Johansson, G.; Bergmark, T.; Karlsson, S. E.; Lindgren, I.; Lindberg, B. *Nova Acta Regiae Soc. Sci. Ups.* **1967**, *20*, 282.
(40) Cranswick, M. A.; Dawson, A.; Cooney, J. J. A.; Gruhn, N. E.; Lichtenberger, D. L.; Enemark, J. H. *Inorg. Chem.* **2007**, *46*, 10639–10646.
(41) Lichtenberger, D. L.; Kellogg, G. E.; Kristofzski, J. G.; Page, D.; Turner, S.; Klinger, G.; Lorenzen, J. *Rev. Sci. Instrum.* **1986**, *57*, 2366.

experimentally determined analyzer sensitivity function versus electron kinetic energy and baseline adjusted for the ionization intensity comparisons in Figure 5.

Solid-State Nuclear Magnetic Resonance. Solid-state NMR experiments were performed on a Bruker Avance-600 spectrometer (14.09 T) operating at 102.76 and 242.95 MHz for ^{75}As and ^{31}P nuclei, respectively. Approximately 10 mg of AsP_3 powder samples were sealed in a glass tube (4 mm o.d.). All ^{31}P and ^{75}As chemical shifts were referenced to 85% H_3PO_4 (aq) and 0.5 M $NaAsF_6$ (in CH_3CN), respectively. The spin−lattice relaxation time (T_1) measurements for ^{31}P were carried out using the inversion recovery method with a recycle delay of 30 s. For ^{75}As, T_1 was determined from the full width at half height (fwhh, $\Delta_{1/2}$), using $T_1 = T_2 = 1/(\pi\Delta_{1/2})$. This assumption was verified by measuring T_1 directly at several temperatures using the saturation recovery method.

Computational Details. The DFT calculations have been carried out using the TURBOMOLE program package[42] version 5.10. The geometries of P_4 and AsP_3 were optimized using the RI-DFT program deck which is utilizing the 'RI two electron integral evaluation routine'. All-electron def2-SV(P) basis sets for both P and As were employed. The electron densities were calculated in terms of gauge independent atomic orbitals (GIAO) using TURBOMOLES mpshift routine. Nonstandard computation criteria used were $denconv 1.0D-7 and $scfconv 6, and an integration grid of m4 quality, The GIMIC input files were generated using TURBOMOLES (hidden) $gimic flag. GIMIC version 2.1[8] was used for the calculation of the current density vectors and their numerical integration.

The closed shell coupled-clusters calculation was performed with MOLPRO version 2008.1[17] at the CCSD(T) level of theory using the explicitly correlated F12b method[43] together with the quadruple-ζ type aug-cc-pCVQZ basis set[44] suitable for including core electron correlation. All electrons were taken into the correlation space. The employed auxiliary basis set for the F12b method was of aug-cc-pwCVQZ/mp2fit[18] type. The geometry was optimized with the MOLPRO numerical gradient method.[2,17]

Acknowledgment. We thank Prof. Kirk A. Peterson (Washington) and MSc Stefan Taubert (Helsinki) for constructive suggestions and discussions, and Dr. Jan J. Weigand (Münster) for providing a purified sample of P_4. D.L.L. thanks the National Science Foundation through the Project CHE-0749530. C.C.C. thanks the National Science Foundation through the Project CHE-719157 and Thermphos International for support. G.W. thanks the Natural Sciences and Engineering Research Council (NSERC) of Canada for support.

Supporting Information Available: GED data analysis parameters for each compound and each data set including R-factors (R_D and R_G), scale factors, correlation parameter values, data ranges, weighting points, nozzle-to-plate distances, and electron wavelengths; complete reference 17. This material is available free of charge via the Internet at http://pubs.acs.org.

JA102580D

(42) Ahlrichs, R.; Bar, M.; Häser, M.; Horn, H.; Kolmel, C. *Chem. Phys. Lett.* **1989**, *162*, 165–169.
(43) Adler, T. B.; Knizia, G.; Werner, H. J. *J. Chem. Phys.* **2007**, *127*, 2211061–2211064.
(44) DeYonker, N. J.; Peterson, K. A.; Wilson, A. K. *J. Phys. Chem. A* **2007**, *111*, 11383–11393.